J Exp Biol Advance Online Articles. First posted online on 1 December 2014 as doi:10.1242/jeb.113522
Access the most recent version at http://jeb.biologists.org/lookup/doi/10.1242/jeb.113522

Nitric oxide production and sequestration in the sinus gland of the green shore crab, *Carcinus maneas*

Natalie L. Pitts and Donald L. Mykles*

Department of Biology, Colorado State University, Fort Collins, CO 80523 USA

Running title: Nitric oxide production in the sinus gland

Key words: nitric oxide, nitric oxide synthase, sinus gland, eyestalk ganglia, copper fluorescent ligand, confocal microscopy, tissue distribution, protein expression, Brachyura, Crustacea, Arthropoda

*Corresponding author:

Dr. Donald L. Mykles
Department of Biology
Colorado State University
Campus Delivery 1878
Fort Collins, CO 80523 USA
Office: 970-491-7616
Fax: 970-491-0649
E-mail: Donald.Mykles@ColoState.edu

Abstract

Molting in decapod crustaceans is regulated by molt-inhibiting hormone (MIH), a neuropeptide produced in the X-organ (XO)/sinus gland (SG) complex of the eyestalk ganglia (ESG). Pulsatile release of MIH from the SG suppresses ecdysteroidogenesis by the molting gland or Y-organ (YO). The hypothesis is that nitric oxide (NO), a neuromodulator that controls neurotransmitter release at presynaptic membranes, depresses the frequency and/or amount of MIH pulses to induce molting. NO synthase (NOS) mRNA was present in *Carcinus maneas* ESG and other tissues and NOS protein was present in the SG. A copper based ligand (CuFL), which reacts with NO to form a highly fluorescent product (NO-FL), was used to image NO in the ESG and SG and quantify the effects of NO scavenger (cPTIO), NOS inhibitor (L-NAME), and sodium azide (NaN_3) on NO production in the SG. Preincubation with cPTIO prior to CuFL loading decreased NO-FL fluorescence ~30%; including L-NAME had no additional effect. Incubating SG with L-NAME during preincubation and loading decreased NO-FL fluorescence ~40%, indicating that over half of the NO release was not directly dependent on NOS activity. Azide, which reacts with NO-binding metal groups in proteins, reduced NO-FL fluorescence to near background levels without extensive cell death. Spectral shift analysis showed that azide displaced NO from a soluble protein in SG extract. These data suggest that the SG contains NO-binding protein(s) that sequester NO and releases it over a prolonged period. This NO release may modulate neuropeptide secretion from the axon termini in the SG.

Introduction

Nitric oxide (NO) is a signaling molecule that is evolutionarily and functionally conserved across animal taxa (Palumbo, 2005). NO is produced by nitric oxide synthase (NOS) from L-arginine, O_2, and NADPH (Colasanti and Venturini, 1998). Three NOS isoforms occur in mammalian cells: endothelial (eNOS), neuronal NOS (nNOS), and inducible NOS (iNOS) (Nathan and Xie, 1994; Bogdan, 2001; Mungrue et al., 2003). eNOS and nNOS are constitutively expressed and require Ca^{2+} and calmodulin for activation (Roman et al., 2002). iNOS is a Ca^{2+} independent isoform that is up regulated during immunological responses (Colasanti and Venturini, 1998). Decapod crustacean tissues express a single NOS that resembles the Ca^{2+}/calmodulin-dependent isoforms in functional domains and biochemical properties (Johansson and Carlberg, 1994; Lee et al., 2000; Scholz et al., 2002; Zou et al., 2002; Kim et al., 2004; McDonald et al., 2011). The crustacean NOS gene is expressed in many tissues, which is consistent with its role as a regulator of diverse physiological functions (Lee et al., 2000; Kim et al., 2004; Inada et al., 2010; Yao et al., 2010; McDonald et al., 2011; Li et al., 2012; Wu et al., 2013).

In the central nervous systems (CNS) of vertebrates and invertebrates, NO functions as a neuromodulator. In vertebrates, NO regulates learning, memory, feeding, sleeping, sensory, and motor functions by acting as an inhibitor or enhancer of neurotransmitter release (Calabrese et al., 2007; Garthwaite, 2008; Virarkar et al., 2013). For example, NO enhances acetylcholine release in the basal forebrain and ventral striatum and inhibits histamine release in the anterior hypothalamus (Philippu and Prast, 2001). In the vertebrate hippocampus and cerebral cortex, NO plays a dual role in the regulation of glutamate release, acting as an inhibitor at low concentrations and a stimulator at high concentrations (Sequeira et al., 1997). In addition, NO has neurotoxic effects that are associated with neurodegenerative disorders, such as Alzheimer's, Parkinson's, and Huntington's diseases (Calabrese et al., 2007; Lorenc-Koci and Czarnecka, 2013; Virarkar et al., 2013;.see Hirst and Robson, 2011 and Russwurm et al., 2013 for comprehensive reviews of NO actions in vertebrates). In decapod crustaceans, NO acts as an enhancer or inhibitor by increasing neurotransmitter release in the stomatogastric ganglion and depressing release in neuromuscular junctions, respectively (Scholz, 1999; Aonuma et al., 2000, 2002).

NO signaling regulates molting and developmental timing in arthropods. In insects, prothoracicotropic hormone (PTTH)-induced stimulation of the molting gland (prothoracic gland or PG) requires NOS activation (Caceres et al., 2011; Rewitz et al., 2013). In the molting gland or Y-organ (YO) of the blackback land crab *Gecarcinus lateralis*, NO donors and YC-1, an agonist of NO-dependent guanylyl cyclase (GC-I), inhibit ecdysteroidogenesis in YO and NOS becomes phosphorylated in the activated YO, which suggests that NOS and GC-I are components of a signaling pathway activated by molt-inhibiting hormone [MIH (Mykles et al., 2010; Chang and Mykles, 2011; Covi et al., 2012)]. MIH is a neuropeptide that represses the YO to maintain the animal in the intermolt stage; a reduction in MIH release is believed to result in the de-repression of steroidogenesis by the YO (Skinner, 1985; Lachaise et al., 1993; Chang and Mykles, 2011). MIH is synthesized in the X-organ (XO), which consists of a cluster of ~150 neurosecretory cells located in the medulla terminalis (MT) of the eyestalk ganglia (Skinner, 1985; Hopkins, 2012). Axons from the XO terminate in the sinus gland (SG), a neurohemal organ where MIH and other XO neuropeptides are released into the hemolymph (Skinner, 1985; Stuenkel, 1985; Hopkins, 2012). The SG consists of glial cells, axons, and axon terminals (Azzouna and Rezig, 2001). NOS protein is localized to the SG of the crayfish, *Procambarus clarkii*, which is suggestive of a role in neuroendocrine regulation (Lee et al., 2000).

The regulation of neuropeptide synthesis and release by the XO/SG complex is poorly understood. mRNA levels of MIH and crustacean hyperglycemic hormone (CHH) in the ESG remain unchanged throughout the molt cycle in *Carcinus maenas*, indicating that MIH and CHH are regulated post-transcriptionally [(Chung and Webster, 2003); N. L. Pitts and D. L. Mykles, unpublished]. The MIH neurons in the XO/SG complex are under serotonergic control (Rudolph and Spaziani, 1991) and neuropeptide release is triggered by entry of Ca^{2+} (Cooke, 1985). The purpose of this study was to examine the potential role of NO signaling in the XO/SG complex of the green shore crab, *C. maenas*. Endpoint RT-PCR was used to determine the expression of *Cm-NOS* and *Cm-Elongation Factor-2 (EF2)* in the eyestalk ganglia and other tissues. The presence of NOS protein in the SG was determined by Western blot analysis. CuFL, a copper (II) fluorescein-based ligand (Lim et al., 2006), was used to localize NO and quantify the effects of NOS inhibitor (L-NAME), NO scavenger (cPTIO), or both compounds on NO production in the SG. The effect of sodium azide (NaN_3), which reacts with heme and other metal groups, on NO-FL fluorescence was quantified. An azide-dependent spectral shift analysis characterized NO-

binding protein(s) in SG soluble extract. The results indicate that NO produced by NOS binds to an endogenous store, allowing for prolonged release of the gas to the axon terminals of the SG. To our knowledge, this is the first study using CuFL to quantify and image NO in crustacean tissues and to characterize NO-binding protein(s) in the SG.

Results

Tissue expression of Cm-NOS

The tissue distribution of *Cm-NOS* was assessed by end point PCR in tissues from a single red color morph intermolt male. *Cm-NOS* mRNA was detected in all tissues examined, except the heart and hepatopancreas (Fig. 1). *Cm-EF2* was expressed in all tissues (Fig. 1).

Detection of NOS protein by Western blotting

NOS protein was present in the SG, as shown by Western blotting with a universal NOS antibody (Fig. 2). An immunoreactive protein of the predicted molecular weight (~132 kDa) was detected with the primary antibody (Fig. 2, lane a). A second protein with an estimated mass of 94 kDa may represent a truncated NOS isoform (see Discussion). Based on scanning densitometry, the level of the ~94-kDa protein was about 2-fold greater than the level of the ~132-kDa protein.

Imaging and quantification of NO-FL fluorescence

NO was quantified with CuFL. NO reacts with CuFL to form NO-FL, a highly fluorescent product that becomes trapped in the cells (Lim et al., 2006). The CuFL concentration used in the experiments was optimized by loading SG with 10-fold serial dilutions between 0.5 mM and 0.05 µM CuFL in the presence or absence of the NO scavenger cPTIO or the NOS inhibitor L-NAME. Loading time was 1 h. NO-FL was highly fluorescent at higher concentrations (> 5 µM), which saturated the tissue and obscured imaging tissue structure with confocal microscopy. A concentration of 0.05 µM was selected, as at that concentration background fluorescence was minimized, while the effects of cPTIO and/or L-NAME on fluorescent intensity could be quantified with Metamorph imaging software.

Confocal microscopy of the NO-FL fluorescence confirmed that NO was produced in the SG *in situ*. ESG was preincubated in crab saline for 30 min and then loaded with 0.05 µM CuFL

for 1 h in the dark. NO-FL fluorescence intensity was greater in the SG compared to the surrounding medulla interna [MI (Fig. 3, left panel)]. In bright field images, the SG appeared dark due to the accumulation of neuropeptide secretory vesicles in axon termini (Fig. 3, middle panel). NO-FL fluorescence in the isolated SG was comparable to that of the *in situ* SG (see Fig. 4B), indicating that the fluorescence in the isolated SG was not an artifact of dissection. The pattern of NO-FL fluorescence indicated that NO was produced in glial and other supporting cells and not in axon termini.

The effects of reagents on NO-FL fluorescence were determined on the isolated SG. Initial experiments examined the effects of pretreatment conditions and also confirmed that NO was produced in the SG. Although the relative NO-FL fluorescence varied between individuals, there was no difference in fluorescence between the two SG from the same individual (data not shown). SG were preincubated in the dark for 30 min in crab saline, 1 mM cPTIO, or 1 mM cPTIO + 1 mM L-NAME, followed by loading for 1 h in the dark with or without 0.05 µM CuFL. SG loaded without CuFL had less than 5% of the fluorescence ($p = 0.002$) compared to SG loaded with CuFL after preincubation in crab saline, showing that the fluorescence was specific for NO-FL and not due to tissue autofluorescence (Fig. 4A). Representative confocal images show the absence of fluorescence in a SG without CuFL (Fig. 4B, panel 1), compared with high fluorescence in a SG with CuFL (Fig. 4B, panel 2). Preincubation with cPTIO alone or in combination with L-NAME reduced NO-FL fluorescence 35% and 26%, respectively, compared to the saline pretreatment control (Fig. 4A). Corresponding confocal images showed a general overall reduction in fluorescence in SG preincubated with cPTIO or with cPTIO + L-NAME (Fig. 4B, compare panels 3 & 4 with panel 2). The reduction in fluorescence appeared to be solely the result of cPTIO, as the addition of L-NAME during preincubation did not decrease fluorescence further. This unexpected result suggested that there was significant NO production and/or release during the 1-h loading period. These results showed that the NO concentrations in the SG were within the linear response range at the concentration of CuFL used, and that CuFL was a highly sensitive and specific reagent for localizing and quantifying NO in crustacean tissues.

A second set of experiments examined the effects of cPTIO and L-NAME when in direct competition with CuFL during the loading period. The experiments followed a similar protocol: isolated SG were preincubated in the dark for 30 min in crab saline, 1 mM cPTIO and/or 1 mM

L-NAME, followed by loading for 1 h in the dark with 0.05 µM CuFL in crab saline with or without 1 mM cPTIO or 1 mM L-NAME. SG preincubated in saline and then incubated with cPTIO and CuFL during loading had a 23% increase ($p = 0.047$) in fluorescence intensity than the control SG without cPTIO (Fig. 5A). A similar trend was also observed when SG were preincubated with cPTIO, but the difference was not significant (Fig. 5A). This suggested that CuFL had a higher NO binding affinity and thus was a better scavenger of free NO than cPTIO. This is particularly striking, considering the 20,000-fold difference in concentration between cPTIO (1 mM) and CuFL (0.05 µM). As shown in the first set of experiments, the NO-FL fluorescence was similar in SG preincubated with cPTIO alone and SG preincubated with cPTIO + L-NAME (Fig. 5A, compare columns #2 and #3). Representative confocal images showed similar reductions in NO-FL fluorescence (Fig. 5B, compare panels #2 and #3 with panel #1). Preincubation with cPTIO and L-NAME followed by L-NAME during the CuFL loading period decreased NO-FL fluorescence 40% ($p < 0.001$) compared to the fluorescence without L-NAME in the loading solution (Fig. 5A and 5B, compare panel #4 with panel #3). However, the fluorescence in the continuous presence of L-NAME in the preincubation and loading periods was well above the baseline level (Fig. 5A and Fig. 5B, panel #4), which suggested that more than half of NO-FL fluorescence was not directly dependent on NOS activity.

Effects of azide on NO-FL fluorescence and spectral shift analysis

The failure of an NOS inhibitor and an NO scavenger to completely knock down NO-FL fluorescence suggested that a proportion of the NO was bound by an endogenous protein(s), thus preventing its rapid degradation. A variety of metalloproteins, including heme- and copper-centered proteins, bind NO (Cooper, 1999; Wilson and Torres, 2004). During loading, the CuFL would react with the NO as it was released from the metal group(s). In order to test this hypothesis, SG were preincubated with 1 mM NaN_3; azide binds nearly irreversibly with metal groups and dislodges bound gases, such as O_2, CO_2, H_2S, and NO (Martin et al., 1990). NaN_3 was restricted to the preincubation period, as it would react with CuFL during the loading period and quench fluorescence. Isolated SGs were preincubated in saline containing cPTIO and L-NAME with and without NaN_3, followed by L-NAME during the loading period to minimize *de novo* NO production by NOS. NaN_3 reduced NO-FL fluorescence 57% ($p = 0.033$) compared to the control without NaN_3 (Fig. 5A; compare columns #4 and #5). This reduction was in addition

to the decreased NO-FL fluorescence with L-NAME, resulting in a fluorescent intensity approaching that without CuFL (Fig. 4A, column #1). A representative confocal image shows low NO-FL fluorescence, comparable to the images of SG not loaded with CuFL (compare Fig. 5B, panel #5, with Fig. 4B, panel #1). These data suggest that an endogenous protein(s) binds NO, which was dissociated from the protein with azide.

The reduction of NO-FL fluorescence by azide was not associated with massive cell death. Azide disrupts aerobic respiration; the reduced ATP production could affect cell viability. Thus, the decrease in NO-FL fluorescence could be caused by the loss of NO-FL from dead cells and not from the release of NO from an endogenous store. A cell viability stain was used to image live and dead cells in SG incubated in crab saline (negative control), 1 mM NaN_3, or 70% methanol (positive control) for 30 min. The SG was stained with propidium iodide (PI), which preferentially stained nuclei of dead cells, followed by Hoechst stain, which stained nuclei of all cells. In false-color images with PI in green and Hoechst in red, the nuclei of dead cells appeared orange to yellow when the images were overlayed (Fig. 6). The numbers of dead and live cells were counted by seven naïve observers and the dead:live ratio was calculated for each treatment. All seven observers counted cells from the same images. There was no significance difference in the ratios between observers ($p = 0.666$). The SG incubated in crab saline had the lowest number of dead cells, with a 1.44 ± 0.42 dead:live ratio (Fig. 6, left panels). By contrast, in the SG incubated in 70% methanol (MeOH), the PI and Hoechst staining almost completely overlapped, resulting in an 11.38 ± 1.83 dead:live cell ratio; this is equivalent to 89% of all nuclei stained with PI and Hoechst (Fig. 6, right panels). Azide increased the dead:live cell ratio to 2.66 ± 0.73 (Fig. 6, central panels). The dead:live cell ratio was significantly different among all three treatments: control *vs.* azide ($p = 0.038$), control *vs.* MeOH ($p < 0.001$), and azide *vs.* MeOH ($p = 0.002$).

In order to characterize the NO binding protein(s), a spectral shift analysis was conducted on SG soluble extract. Spectra from 190 nm to 1100 nm at 1-nm resolution were recorded of SG extract prior to and immediately after the addition of 1 mM NaN_3 (Fig. 7; top panel), and at 5-min intervals following the addition of NaN_3 over 1 h (Fig. 7; bottom panel). Differences in spectral peaks were calculated by subtracting the spectra at each 5 min time interval from the spectrum prior to the addition of NaN_3. No spectral shifts were observed in the ranges expected for heme binding (400 nm - 450 nm) or copper binding (600 nm - 700 nm) proteins. In the long

UV range (210 to 450 nm), there was an increase in absorption centered broadly at ~234 nm and a reduction in absorption centered broadly at ~272 nm, relative to the untreated sample (Fig. 7). The absorption changes in these specific regions were completed within the first 5 minutes after the addition of NaN_3, although there was a general drift in absorption as the protein precipitated from solution.

Discussion

NO is an important signaling molecule that mediates numerous physiological processes, such as neuromodulation, endocrine regulation, olfaction, and muscle contraction/relaxation (Radomski et al., 1991; Martinez et al., 1994; Hurst et al., 1999; Bishop and Brandhorst, 2001). The distribution of NOS in nervous and other tissues is consistent with diverse roles of NO in decapod crustaceans [Fig. 1; (Kim et al., 2004; McDonald et al., 2011)]. The *C. maenas* SG expressed a full-length NOS protein with a mass predicted from the cDNA sequence [~132 kDa; Fig. 2 (McDonald et al., 2011)]. The observed ~94-kDa protein on the Western blot may represent an uncharacterized truncated NOS isoform in the SG of *C. maenas* (Fig. 2). In *Drosophila melanogaster*, for example, NOS isoforms ranging in mass between 22 kDa and 151 kDa are generated by alternative splicing and alternative start sites and some truncated isoforms act as dominant negative regulators (Regulski and Tully, 1995; Stasiv et al., 2001). In arthropods, NO production has largely been inferred from NOS localization using immunohistochemistry or NADPH diaphorase histochemistry on fixed tissues (Scholz et al., 1998; Scholz et al., 2002; Zou et al., 2002; Kim et al., 2004; Mahadevan et al., 2004; Yeh et al., 2006; Ott et al., 2007; McDonald et al., 2011). 4,5-Diaminofluorescein-2 (DAF-2) was used to detect NO in the terminal abdominal ganglion of the crayfish, *Pacifastacus leniusculus* and hemocytes in the tiger shrimp, *Penaeus monodon* (Schuppe et al., 2002; Wu et al., 2013). The present study used CuFL to localize and quantify NO production in the eyestalk ganglia and SG. The major findings are: (1) CuFL is a highly specific and sensitive probe for NO in crustacean tissue; (2) NO production in the *C. maenas* SG requires NOS activity; and (3) endogenous protein(s) sequesters NO and releases NO over a prolonged period.

CuFL is a highly specific cell-permeable probe for NO in living cells (Lim et al., 2006; McQuade et al., 2010; Gusarov et al., 2013). In order to establish that the fluorescence observed after CuFL loading was NO-dependent, NOS inhibitor (L-NAME) and NO scavenger (cPTIO)

were used to reduce NO-FL fluorescence in the SG. Preincubation with cPTIO or cPTIO + L-NAME decreased NO-FL fluorescence by ~30% (Fig. 4). Including L-NAME during CuFL loading decreased fluorescence by 40% (Fig. 5), indicating that more than half of the NO-FL fluorescence was not directly dependent on NOS activity. As NO has a half-life on the order of seconds in aerated aqueous solutions (Moncada et al., 1991), the gas was apparently bound by an endogenous protein, which released NO over the 1 h loading period. In the salivary glands of several blood sucking insects, such as *Rhodnius prolixus* (Ribeiro et al., 1993), *Cimex lectularius* (Weichsel et al., 2005), and *Triatoma infestans* (Assumpcao et al., 2008), NO is sequestered by heme proteins. NO is reversibly bound to an Fe(III) heme protein that releases NO when exposed to a neutral pH at the site of the wound. We hypothesized that NO was sequestered in a similar manner in the SG of *C. maenas*. In order to test this hypothesis, 1 mM NaN_3 was added during preincubation to drive the dissociation of NO from a protein to which it was bound. This resulted in a further 57% reduction in fluorescence compared to SGs preincubated with cPTIO + L-NAME without NaN_3 (Fig. 5), supporting the hypothesis that NO was bound by an endogenous protein. To determine that the large reduction in NO-FL fluorescence by NaN_3 was not the result of large-scale cell death, we used a propidium iodide cell viability stain to quantify the dead:live cell ratio in SG incubated in saline, 1 mM NaN_3 in saline, or 70% MeOH for 30 min. SG treated with azide had a 1.8-fold increase in dead cells compared to SG treated with crab saline (Fig. 6). This compares with a 7.2-fold difference in NO-FL fluorescence between SG incubated with or without azide (Fig. 5A, compare column #1 to #5). Thus, the increased cell death with azide accounts for no more than 13% of the decrease in NO-FL fluorescence with azide.

To further characterize this protein, a spectral shift analysis was performed on a soluble extract of isolated SGs in the presence of NaN_3. An azide-dependent dissociation of NO from a heme group would cause a negative spectral shift in the Soret peak [400 nm- 450 nm; see (Ribeiro et al., 1993)]. No spectral shift was observed in this range, indicating the NO-binding moiety was not a heme group (Fig. 7). Alternatively, if an NO bound to a copper-containing protein is displaced by NaN_3, we would expect a negative spectral shift in the 600 nm – 700 nm range (Wilson and Torres, 2004). By contrast, azide caused a positive spectral shift in the 225 nm – 245 nm range and a negative shift in the 245 nm – 290 nm range. Further analysis is needed to identify the NO-binding protein(s) involved. Nevertheless, the spectral shift analysis showed that the SG contains an endogenous NO storage protein, but the moiety that bound NO

was not a heme or copper group. Absorption at ~272 nm is typical of phenylalanine, tyrosine, and tryptophan side chains, which may suggest the formation of azidoadducts of aromatic amino acids. p-Azidophenylalanine adducts of dihydrofolate reductase show an increased absorption at ~250 nm (Carrico, 2004) compared to the unmodified enzyme, while 6-azidotryptophan shows an absorption at 248 nm that is not present in unmodified tryptophan (Miles and Phillips, 1985). The data indicate that azide displaces NO from a metal-containing protein(s), which is associated with the reaction of azide with aromatic side chains.

CuFL was a better scavenger of NO than cPTIO. When cPTIO and CuFL were in direct competition during the loading period, there was no decrease in NO-FL fluorescence in the SG by cPTIO. Surprisingly, the fluorescent intensity was increased moderately (Fig. 5A), compared to loading with CuFL alone. The concentration of cPTIO was 20,000 times greater than CuFL (1 mM *vs.* 0.5 µM, respectively), suggesting that the increase in fluorescence observed when cPTIO and CuFL were loaded together was a result of the CuFL being a more efficient NO scavenger than cPTIO. This is consistent with results from experiments that included cPTIO during preincubation and loading. cPTIO alone during preincubation could effectively scavenge NO and reduce NO-FL fluorescence (Fig. 4). However, when CuFL was added to the cPTIO solution during loading, fluorescence increased or did not change (Fig. 5), indicating that CuFL outcompeted cPTIO for binding to free NO. Similar results were found when DAF-2 was used to quantify NO in plant tissues; at high NO levels cPTIO increased DAF-2 NO fluorescence (Vitecek et al., 2008). This effect was attributed to DAF-2 binding to N_2O_3, a byproduct of the reaction of cPTIO and NO. However, CuFL does not react with N_2O_3. An alternative explanation is that cPTIO reacts with cellular substrates, such as reductases, which prevents it from scavenging NO (Haseloff et al., 1997). The high affinity of CuFL for NO makes it an excellent NO probe for use in living tissues, even in the presence of NO scavengers.

Figure 8 is a schematic diagram that summarizes the reactions and the effects of reagents during the preincubation and loading conditions. It is assumed that all the NO in the SG is produced by NOS. Some of the NO binds reversibly to endogenous protein (XX-NO), while some binds reversibly to GC-I and other NO-dependent enzymes (not included in the diagram). cPTIO acts as an NO scavenger by converting NO to NO_2, which can react with NO to form N_2O_3. CuFL reacts with NO to form NO-FL and Cu(I). As CuFL has a higher affinity for NO than cPTIO, the formation of NO-FL is favored over the formation of NO_2 when both reagents

are present during loading. Azide reacts with the protein (N_3XX) and the released NO reacts with water to form nitrite and nitrate. As preincubation with cPTIO or with cPTIO + L-NAME does not affect NO release from endogenous proteins during CuFL loading, NO-FL fluorescence is reduced but not completely eliminated. The largest reduction in NO-FL fluorescence is achieved when the SG is preincubated with NaN_3, cPTIO, and L-NAME. NaN_3 drives the release of NO from endogenous stores and the NO reacts with cPTIO. L-NAME inhibits NOS and prevents NO production during the preincubation period, as well as during the CuFL loading period.

Confocal microscopy revealed that NO-FL distribution was not uniform. Images of the SG *in situ* (Fig. 3), as well as of the isolated SG (Figs. 4, 5), showed that NO-FL fluorescence was preferentially located in cells that surrounded and penetrated the SG. The variation in NO-FL fluorescence was not due to variations in the size and thickness of the tissue. As areas of strong fluorescence occurred throughout the optical sections of the z-stack, the 1 h loading period was sufficient time for the CuFL to penetrate to the interior of the SG. The SG is structured as a network of groups swollen axon termini separated by glial cell projections (Fu et al., 2005). This is apparent in the cell viability images, in which the nuclei of glial and other supporting cells surround axon termini that lack nuclei (Fig. 6). The distribution of NO-FL is consistent with the production of NO by supportive tissues containing glial cells (Figs. 3, 4B, and 5B). We conclude that the site of NO production, storage, and release is confined to supportive structures and areas within the SG lacking NO-FL fluorescence are axon termini. Additionally, several terminal types are present in the SG (Fu et al., 2005), therefore areas of NO-FL fluorescence may identify supportive cells near terminals from which neuropeptide release is NO dependent and terminals adjacent to areas lacking NO-FL rely on another mechanism for peptide release.

As MIH transcript levels remain constant over the molt cycle, MIH synthesis and secretion are regulated by post-transcriptional mechanisms [(Chung and Webster, 2003); N.L. Pitts and D.L. Mykles, unpublished]. NO inhibits neuropeptide release in the hippocampus, bovine chromaffin cells, basal forebrain, and nucleus accumbens in the mammalian brain (Sequeira et al., 1997; Schwarz et al., 1998; Philippu and Prast, 2001). As NO is produced rapidly and quickly diffuses across cell membranes, we propose that variations in NO release provide a mechanism for regulating the pulsatile release of MIH. If NO inhibits MIH secretion from the SG, then it follows that NO synthesis and release should vary with molt stage: it should be highest during premolt and postmolt stages and lowest during intermolt. There is measureable

NO production in SG of intermolt animals, but other molt stages were not examined (Fig. 3, 4, 5). The amount of NO released is determined by NOS activity and/or NO sequestration. The experiments with cPTIO and L-NAME showed that about 60% of the NO-FL fluorescence during the loading period was from the release of NO from an endogenous storage protein (Figs. 4, 5). Sequestration of NO during intermolt would reduce NO release, resulting in elevated MIH secretion from the SG. The higher frequency and amount of MIH release would keep the YO in the basal state (Chung and Webster, 2003; Mykles et al., 2010; Chang and Mykles, 2011; Covi et al., 2012). The hypothesis predicts that NO release increases during premolt, resulting from increased NOS activity, decreased NO sequestration, or a combination of the two. Future work will address this question by measuring total NO-FL fluorescence, as well as the contribution of the NO storage protein to total NO-FL fluorescence, in the SG from intermolt, premolt, and postmolt animals.

In summary, the SG is a site of higher NO production in the ESG of intermolt *C. maenas*. As a highly specific and sensitive indicator of NO, CuFL is an effective probe for NO production in living cells. CuFL readily penetrates tissues and reacts with NO to form NO-FL, making it a more effective NO scavenger than cPTIO. NO-FL is highly fluorescent, requiring very low concentrations (0.05 µM) of CuFL, which minimizes non-specific and possible toxic effects. NO-FL is stable at neutral pH, which allows for the quantification and localization of NO over a period of several hours. To our knowledge, this is the first report using CuFL to image and measure NO in crustacean tissues. The effects of azide, cPTIO, and L-NAME on NO-FL fluorescence indicate that greater than half of the NO synthesized by NOS was sequestered by an endogenous storage protein. Azide-dependent spectral shift analysis of SG soluble extract indicated that NO was bound to a metal-containing protein, but the metal is not iron or copper. The localization of NOS and NO-FL to supportive tissues suggests that NO produced and released by glial cells modulates neuropeptide secretion from axon terminals. The episodic release of MIH may be regulated by a NO/cGMP-dependent feedback mechanism. NO sequestration during intermolt may dampen the feedback mechanism, thus increasing MIH pulses to maintain the YO in the basal state during intermolt (Mykles et al., 2010; Chang and Mykles, 2011; Covi et al., 2012). Increased NO release due to increased NOS activity and/or decreased NO sequestration enhances the negative feedback loop. Consequently, the reduction in

MIH pulses drives the transition of YO from the basal to activated state and the animal enters premolt.

Materials and Methods

Animals

Green shore crabs were collected from Bodega Harbor in Bodega Bay, California. They were maintained under ambient conditions in a flow-through sea water system (12-15 °C) at Bodega Marine Laboratory (Abuhagr et al., 2014). Only intermolt (stage C_4) adult male crabs were used. Molt stage was determined by hemolymph ecdysteroid concentrations and the presence or absence of the membranous layer in the exoskeleton (Abuhagr et al., 2014). Ecdysteroids were quantified using a competitive enzyme-linked immunoassay (Kingan, 1989; Abuhagr et al., 2014).

End-point PCR

Tissue expression of *Cm-NOS* (GenBank accession #GQ862349) was determined using end-point RT-PCR. *Cm-EF2* (GenBank accession #GU808334) is a constitutively expressed gene and served as a control to assess the quality of RNA isolations and cDNA synthesis. RNA was isolated from tissues of an intermolt male *C. maenas* using TRIzol reagent (Life Technologies, Carlsbad, CA USA) according to the manufacture's protocol. Total RNA was treated with DNase I (New England Biolabs, Ipswich, MA USA) followed by a phenol:chloroform extraction. RNA was precipitated overnight in a 3:1 mixture of isoamyl alcohol:sodium acetate (pH 5.2) and re-suspended in 20 µL nuclease free water. RNA was reverse transcribed with Transcriptor Reverse Transcriptase (Roche Diagnostics, Indianapolis, IN USA) and an oligo-dT primer (50 µmol). PCR reactions contained 1 µL template cDNA, 0.5 µL 10 µM forward primer (*Cm-NOS*, 5'-GTG TGG AAG AAG AAC AAG GAC C-3'; *Cm-EF2*, 5'-CCA TCA AGA GCT CCG ACA ATG AGC G-3'), 0.5 µL 10 µM reverse primer (*Cm-NOS*, 5'-TCT GTG GCA TAG AGG ATG GTG G-3'; *Cm-EF2*, 5'-CAT TTC GGC ACG GTA CTT CTG AGC G-3'), 5 µL 2x PCR master mix (Thermo Scientific, Rockford, IL USA), and 3 µL sterile deionized water. Primers were synthesized by Integrative DNA Technologies (Coralville, IA USA). PCR conditions were as follows: 5 min denaturation at 95 °C, 35 cycles of 30 sec denaturation at 95 °C, 30 sec annealing at 58 °C (*Cm-NOS*) or 61 °C (*Cm-EF2*), 30 sec extension

at 72 °C, and final extension at 72 °C for 7 min. Products were separated on a 1.5% agarose gel and stained with ethidium bromide.

Western Blot Analysis

Twelve SG were homogenized in 150 µL buffer containing 20 mM Tris-HCl (pH 7.4), 1 mM EDTA, 20 mM KCl, and 10% protease inhibitor cocktail (Sigma Aldrich, St. Louis, MO USA) for 5 min and centrifuged at 30,000 g for 15 min. A sample of the supernatant fraction (24 µL; 50 µg protein) was combined with 8 µL sodium dodecyl sulfate-polyacrylamide gel electrophoresis (SDS-PAGE) sample buffer (Bio-Rad Laboratories, Inc., Hercules, CA USA) and incubated at 95 °C for 10 min. SG protein samples and SeeBlue Plus 2 pre-stained standard (Invitrogen, Carlsbad, CA USA) were separated by SDS-PAGE (200V, 30 min) on a Mini-Protean TGX 4-15% Tris-glycine gel (Bio-Rad Laboratories, Hercules, CA USA) using a Tris-glycine buffer system. Proteins were transferred to a polyvinylidene difluoride (PVDF) membrane (100 V, 1 h) and incubated in Tris-buffered saline + Tween-20 (TTBS) plus 2% goat serum (Vector Laboratories, Inc., Burlingame, CA USA) for 45 min at room temperature (RT), followed by an overnight incubation in a 1:100 dilution of the anti-universal NOS antibody (PA1-38835; Pierce Antibodies, Thermo Scientific, Rockford, IL USA) or 2% goat serum (control without primary antibody). The anti-universal NOS antibody recognized a highly conserved peptide sequence (QKRYHEDIFG) in NOS proteins from various species, including *C. maenas* (McDonald et al., 2011). Proteins were incubated with a goat anti-rabbit biotinylated secondary antibody in TTBS for 1 h at RT, followed by 30 min at RT in Vectastain ABC reagent (both from Vector Laboratories, Burlingame, CA USA). The membrane was developed with WesternBright Sirius chemiluminescent HRP substrate (Advansta, Menlo Park, CA USA) according to kit instructions. Images were obtained using a ChemiDoc XRS+ Molecular Imager (Bio-Rad Laboratories, Hercules, CA USA). Band intensities from the Western Blot analysis were measured with Image Lab software (Bio-Rad Laboratories, Hercules, CA, USA).

Imaging and quantification of NO-FL fluorescence

NO was imaged in live cells using Cu-FL, a cell-permeable Cu (II) fluorescein-based ligand, which was made by combining $CuCL_2$ and FL (2-{2-chloro-6-hydroxy-5-[2-methylquinolin-8-ylaminomethyl]-3-oxo3H-xanthen-9}); Strem Chemicals, Newburyport, MA USA) in a 1:1

molar ratio (Lim et al., 2006). ESG and SG were dissected in crab saline, preincubated with crab saline or with 1 mM cPTIO (Cayman Chemical, Ann Arbor, MI, USA), and/or 1 mM L-NAME (Cayman Chemical, Ann Arbor, MI, USA), and/or 1 mM NaN_3 in crab saline for 30 min in the dark; and loaded for 1 h with 0.05 µM CuFL in crab saline with or without 1 mM cPTIO or 1 mM L-NAME in the dark. As SG size and fluorescence intensity varied between individuals, one SG of a pair received the control treatment and the other SG received the experimental treatment. The treatments are detailed in the Results. After CuFL loading, tissues were transferred to crab saline and fluorescence intensity (arbitrary units) was quantified on an Olympus BX50WI microscope (excitation 494 nm, emission 519 nm, exposure time 1 sec, 10x) using Metamorph Image Analysis software (Molecular Devices LLC, Sunnyvale, CA USA). A SG was optically divided into 4 quadrants and the average intensity of each image was summed to calculate the total fluorescence intensity for the entire SG. After quantification, SG were imaged with an Olympus Fluoroview FV 500 confocal laser scanning biological microscope (488 nm excitation, 519 nm emission, 10x objective). Images were composites of 20 stacked optical sections. Quantification and imaging of SG pairs was completed less than 2 h after the end of the loading period.

Cell viability imaging

A LIVE/DEAD Sperm Viability Kit (L-7011; Molecular Probes, Eugene, OR, USA) was used to identify live and dead cells in isolated SG. SG were incubated 30 min in crab saline, 70% methanol, or 1 mM NaN_3 in crab saline and stained 5 min with 12 µM propidium iodide in crab saline followed by 10 µM Hoechst 33342 stain (H211492; Molecular Probes, Eugene, OR, USA) in crab saline. SG were imaged with an Olympus Fluoroview FV 500 confocal laser scanning biological microscope (358 nm excitation, 461 nm emission for Hoechst and excitation 494 nm, emission 519 nm for PI with 20x objective) as described above. In false-color images, PI staining was set as green and Hoechst staining was set as red. The ratio of dead to live cells was obtained by counting the number of yellow/orange and red nuclei, respectively, for each treatment by 7 naïve observers. The observers were given the 3 unlabeled overlay images (Fig. 6), as well as a legend showing examples of red, orange, and yellow nuclei. Observers were instructed to count the number of red and yellow/orange cells in each image. The ratio of dead to live cells for each observer was calculated and averaged.

Spectral shift analysis

Thirty SG were homogenized in 2 mL of phosphate buffered saline (137 mM NaCl; 10 mM sodium phosphate, pH, 7.4; and 2.7 mM KCl). Homogenate samples (0.5 mL aliquotes) were flash frozen in liquid nitrogen. On the day of the experiment, samples were thawed on ice and centrifuged at 30,000 g for 15 min at 4˚C to remove cellular debris. Samples were kept in the dark whenever possible. Spectra at 1 nm intervals were recorded with 5 sec integration using an Agilent 8453 diode array spectrophotometer (Agilent Technologies, Inc. Santa Clara, CA USA) from 190 nm to 1100 nm and analyzed using UV-Visible Chemstation Version B.01.01 software (Agilent Technologies, Inc. Santa Clara, CA USA). The cuvette path length was 1 cm and spectra ranged from 0.5 to 1.0 absorbance units across the entire spectral range. Following a baseline measurement, 10 µL 1 M NaN_3 was added directly to the sample and a reading was taken every 5 min for 1 h. Differences in spectra were calculated by subtracting each 5 min time interval after the addition of azide from the baseline measurement before azide.

Statistical analyses and software

Statistical analysis used Sigma Plot 12.0 software (Systat Software Inc., San Jose CA, USA). Differences in mean fluorescent intensities between control and experimental SG used a paired t-test analysis. Differences in dead to live cell ratios between treatment groups and observers used a Kruskal-Wallis analysis (variance on ranks). Data are presented as mean ± 1 s.e. and the level of significance was set at $\alpha = 0.05$. Graphs were constructed in Sigma Plot. All other figures were created using Illustrator and Photoshop 10 (Adobe Systems, San Jose, CA, USA).

Symbols and Abbreviations

cGMP: 3’5’-guanosine monophosphate

CHH: crustacean hyperglycemic hormone

CNS: central nervous system

cPTIO: 2-(4-Carboxyphenyl)-4,4,5,5-tetramethylimidazoline-1-oxyl-3-oxide (NO scavenger)

CuFL: Cu(II) fluorescein based ligand

DAF-2: 4,5-diaminofluorescein-2

EF2: elongation factor 2

ESG: eyestalk ganglia

FL: 2-{2-chloro-6-hydroxy-5-[2-methylquinolin-8-ylaminomethyl]-3-oxo3H-xanthen-9}; fluorescent ligand

GC-I: soluble class I guanylyl cyclase

L-NAME: L-N^G-Nitroarginine methyl ester

MeOH: methanol

MI: medulla interna

MIH: molt inhibiting hormone

MT: medulla terminalis

NADPH: nicotinamide adenine dinucleotide phosphate

NaN_3: sodium azide

NO: nitric oxide

NO_2: nitrogen dioxide

NO_2O_3: dinitrogen trioxide

NO-FL: nitric oxide-fluorescent complex

NOS: nitric oxide synthase; eNOS = endothelial NOS, iNOS = inducible NOS, nNOS = neuronal NOS

PG: prothoracic gland

PTTH: prothoracictropic hormone

PVDF: polyvinylidene difluoride

RT: room temperature

RT-PCR: reverse transcriptase polymerase chain reaction

SDS-PAGE: sulfate-polyacrylamide gel electrophoresis

SG: sinus gland

TTBS: tris-buffered saline + tween

XO: X-organ

YC-1: 5-[1-(phenylmethyl)-1H-indazol-3-yl]-2-furanmethanol; NO independent activator of GC-I

YO: Y-organ

Acknowledgements

We thank Dr. Ernest S. Chang, UC Davis Bodega Marine Laboratory, for manuscript comments and providing laboratory facilities and equipment; Dr. Sukkrit Nimitkul, UC Davis Bodega Marine Laboratory, for animal collection and care and technical assistance; Dr. Gary Cherr, UC Davis Bodega Marine Laboratory, for assistance with the Fluorescence Imaging Facility; and Dr. P. Shing Ho, Colorado State University, for providing equipment and facilities for the spectral shift analysis and for comments on the manuscript.

Funding

This research was supported by a grant from the National Science Foundation to D.L.M. (IOS-1257732) and by travel grants awarded to N.L.P. from The Crustacean Society, The Journal of Experimental Biology Traveling Fellowship, and The Society for Integrative and Comparative Biology Grants in Aid of Research.

Author Contributions

N.L.P and D.L.M. designed the study; N.L.P completed the experiments; and N.L.P. and D.L.M. prepared the manuscript.

Competing Interests

The authors declare no competing financial interests.

References

Abuhagr, A. M., Blindert, J. L., Nimitkul, S., Zander, I. A., LaBere, S. M., Chang, S. A., MacLea, K. S., Chang, E. S. and Mykles, D. L. (2014). Molt regulation in green and red color morphs of the crab *Carcinus maenas*: gene expression of molt-inhibiting hormone signaling components. *J. Exp. Biol.* **217**, 796-808.

Aonuma, H., Nagayama, T. and Takahata, M. (2000). Modulatory effects of nitric oxide on synaptic depression in the crayfish neuromuscular system. *J. Exp. Biol.* **203**, 3595-3602.

Aonuma, H., Nagayama, T. and Takahata, M. (2002). Nitric oxide and cyclic GMP modulate synaptic transmission in the local circuits of the crayfish. In *The Crustacean Nervous System,* (ed. K. Wiese), pp. 305-312. Berlin: Springer.

Assumpcao, T. C. F., Francischetti, I. M. B., Andersen, J. F., Schwarz, A., Santana, J. M. and Ribeiro, J. M. C. (2008). An insight into the sialome of the blood-sucking bug *Triatoma infestans*, a vector of Chagas' disease. *Insect Biochem. Molec. Biol.* **38**, 213-232.

Azzouna, A. and Rezig, M. (2001). Ultrastructural study of the sinus gland of the shrimp *Palaemonetes mesogenitor* Sollaud, 1912. *B. Soc. Zool. Fr.* **126**, 217-219.

Bishop, C. D. and Brandhorst, B. P. (2001). The role of NO/cGMP and HSP90 in regulating metamorphosis of the sea urchin *Lytechinus pictus*. *Dev. Biol.* **235**, 251-251.

Bogdan, C. (2001). Nitric oxide and the regulation of gene expression. *Trends Cell Biol.* **11**, 66-75.

Caceres, L., Necakov, A. S., Schwartz, C., Kimber, S., Roberts, I. J. H. and Krause, H. M. (2011). Nitric oxide coordinates metabolism, growth, and development via the nuclear receptor E75. *Genes Dev.* **25**, 1476-1485.

Calabrese, V., Mancuso, C., Calvani, M., Rizzarelli, E., Butterfield, D. A. and Stella, A. M. G. (2007). Nitric oxide in the central nervous system: neuroprotection versus neurotoxicity. *Nat. Rev. Neurosci.* **8**, 766-775.

Carrico, I. S. (2004). Protein Engineering Through *in vivo* Incorporation of Phenylalanine Analogs. Doctor of Philosophy. Pasadena, CA: California Institute of Technology.

Chang, E. S. and Mykles, D. L. (2011). Regulation of crustacean molting: A review and our perspectives. *Gen. Comp. Endocrinol.* **172**, 323-330.

Chung, J. S. and Webster, S. G. (2003). Moult cycle-related changes in biological activity of moult-inhibiting hormone (MIH) and crustacean hyperglycaemic hormone (CHH) in the crab, *Carcinus maenas* - From target to transcript. *Eur. J. Biochem.* **270**, 3280-3288.

Colasanti, M. and Venturini, G. (1998). Nitric oxide in invertebrates. *Molec. Neurobiol.* **17**, 157-174.

Cooke, I. M. (1985). Electrophysiological characterization of peptidergic neurosecretory terminals. *J. Exp. Biol.* **118**, 1-35.

Cooper, C. E. (1999). Biochemistry of nitric oxide. *Biochim. Biophys. Acta* **1411**, 215-216.

Covi, J. A., Chang, E. S. and Mykles, D. L. (2012). Neuropeptide signaling mechanisms in crustacean and insect molting glands. *Invert. Reprod. Dev.* **56**, 33-49.

Fu, Q., Kutz, K. K., Schmidt, J. J., Hsu, Y. W. A., Messinger, D. I., Cain, S. D., De la Iglesia, H. O., Christie, A. E. and Li, L. J. (2005). Hormone complement of the *Cancer productus* sinus gland and pericardial organ: An anatomical and mass spectrometric investigation. *J. Comp. Neurol.* **493**, 607-626.

Garthwaite, J. (2008). Concepts of neural nitric oxide-mediated transmission. *Eur. J. Neurosci.* **27**, 2783-2802.

Gusarov, I., Gautier, L., Smolentseva, O., Shamovsky, I., Eremina, S., Mironov, A. and Nudler, E. (2013). Bacterial nitric oxide extends the lifespan of *C. elegans*. *Cell* **152**, 818-830.

Haseloff, R. F., Zollner, S., Kirilyuk, I. A., Grigorev, I. A., Reszka, R., Bernhardt, R., Mertsch, K., Roloff, B. and Blasig, I. E. (1997). Superoxide-mediated reduction of the nitroxide group can prevent detection of nitric oxide by nitronyl nitroxides. *Free Radical Res.* **26**, 7-17.

Hirst, D.G. and Robson T. (2011). Nitric oxide physiology and pathology. *Methods in Molec. Biol.* **704**, 1-13.

Hopkins, P. M. (2012). The eyes have it: A brief history of crustacean neuroendocrinology. *Gen. Comp. Endocrinol.* **175**, 357-366.

Hurst, W. J., Moroz, L. L., Gillette, M. U. and Gillette, R. (1999). Nitric oxide synthase immunolabeling in the molluscan CNS and peripheral tissues. *Biochem. Biophys. Res. Commun.* **262**, 545-548.

Inada, M., Mekata, T., Sudhakaran, R., Okugawa, S., Kono, T., El Asely, A. M., Linh, N. T. H., Yoshida, T., Sakai, M., Yui, T. et al. (2010). Molecular cloning and characterization of the nitric oxide synthase gene from kuruma shrimp, *Marsupenaeus japonicus*. *Fish Shellfish Immunol.* **28**, 701-711.

Johansson, K. U. I. and Carlberg, M. (1994). NADPH-diaphorse histrochemistry and nitric oxide synthase activity in deutocerebrun of the crayfish, *Pacifastacus leiusculus* (Crustacea, Decapoda). *Brain Res.* **649**, 36-42.

Kim, H. W., Batista, L. A., Hoppes, J. L., Lee, K. J. and Mykles, D. L. (2004). A crustacean nitric oxide synthase expressed in nerve ganglia, Y-organ, gill and gonad of the tropical land crab, *Gecarcinus lateralis*. *J. Exp. Biol.* **207**, 2845-2857.

Kingan, T. G. (1989). A competitive enzyme-linked immunosorbent assay: application in the assasy of peptides, steroids, and cyclic nucleotides. *Anal. Biochem.* **183**, 283-289.

Lachaise, F., Leroux, A., Hubert, M. and Lafont, R. (1993). The molting gland of crustaceans: localization, activity, and endocrine control (a review). *J. Crustacean Biol.* **13**, 198-234.

Lee, C. Y., Zou, H. S., Yau, S. M., Ju, Y. R. and Liau, C. S. (2000). Nitric oxide synthase activity and immunoreactivity in the crayfish *Procambarus clarkii*. *Neuroreport* **11**, 1273-1276.

Li, S. K., Zhang, Z., Li, C. B., Zhou, L. Z., Liu, W. H., Li, Y. Y., Zhang, Y. L., Zheng, H. P. and Wen, X. B. (2012). Molecular cloning and expression profiles of nitric oxide synthase (NOS) in mud crab *Scylla paramamosain*. *Fish Shellfish Immunol.* **32**, 945-946.

Lim, M. H., Xu, D. and Lippard, S. J. (2006). Visualization of nitric oxide in living cells by a copper-based fluorescent probe. *Nat. Chem. Biol.* **2**, 375-380.

Lorenc-Koci, E. and Czarnecka, A. (2013). Role of nitric oxide in the regulation of motor function. An overview of behavioral, biochemical and histological studies in animal models. *Pharmacol. Rep.* **65**, 1043-1055.

Mahadevan, A., Lappe, J., Rhyne, R. T., Cruz-Bermudez, N. D., Marder, E. and Goy, M. F. (2004). Nitric oxide inhibits the rate and strength of cardiac contractions in the lobster *Homarus americanus* by acting on the cardiac ganglion. *J. Neurosci.* **24**, 2813-2824.

Martin, K. D., Saari, L., Wang, G. X., Wang, T., Parkhurst, L. J. and Klucas, R. V. (1990). Kinetics and thermodynamics of oxygen, CO, and azide binding by the subcomponents of soybean leghemoglobin. *J. Biol. Chem.* **265**, 19588-19593.

Martinez, A., Riverosmoreno, V., Polak, J. M., Moncada, S. and Sesma, P. (1994). Nitric oxide (NO) synthase immunoreactivity in the starfish *Marthasterias glacialis*. *Cell Tiss. Res.* **275**, 599-603.

McDonald, A. A., Chang, E. S. and Mykles, D. L. (2011). Cloning of a nitric oxide synthase from green shore crab, *Carcinus maenas*: A comparative study of the effects of eyestalk ablation on expression in the molting glands (Y-organs) of *C. maenas*, and blackback land crab, *Gecarcinus lateralis*. *Comp. Biochem. Physiol.* **158A**, 150-162.

McQuade, L. E., Ma, J., Lowe, G., Ghatpande, A., Gelperin, A. and Lippard, S. J. (2010). Visualization of nitric oxide production in the mouse main olfactory bulb by a cell-trappable copper(II) fluorescent probe. *Proc. Natl. Acad. Sci. USA* **107**, 8525-8530.

Miles, E. W. and Phillips, R. S. (1985). Photoinactivation and photoaffinity labeling of tryptophan synthase alpha-2 beta-2 complex by the product analog 6-azido-L-tryptophan. *Biochem.* **24**, 4694-4703.

Moncada, S., Palmer, R. M. J. and Higgs, E. A. (1991). Nitric oxide; physiology, pathophysiology, and pharmacology. *Pharmacol. Rev.* **43**, 109-142.

Mungrue, I. N., Bredt, D. S., Stewart, D. J. and Husain, M. (2003). From molecules to mammals: what's NOS got to do with it? *Acta Physiol. Scand.* **179**, 123-135.

Mykles, D. L., Adams, M. E., Gade, G., Lange, A. B., Marco, H. G. and Orchard, I. (2010). Neuropeptide action in insects and crustaceans. *Physiol. Biochem. Zool.* **83**, 836-846.

Nathan, C. and Xie, Q. W. (1994). Nitric oxide synthases: roles, tolls, and controls. *Cell* **78**, 915-918.

Ott, S. R., Aonuma, H., Newland, P. L. and Elphick, M. R. (2007). Nitric oxide synthase in crayfish walking leg ganglia: Segmental differences in chemo-tactile centers argue against a generic role in sensory integration. *J. Comp. Neurol.* **501**, 381-399.

Palumbo, A. (2005). Nitric oxide in marine invertebrates: A comparative perspective. *Comp. Biochem. Physiol.* **142A**, 241-248.

Philippu, A. and Prast, H. (2001). Role of histaminergic and cholinergic transmission in cognitive processes. *Drug News Perspect.* **14**, 523-529.

Prast, H. and Philippu, A. (1992). Nitric oxide releases acetylcholine in the basal forebrain. *Eur. J. Pharmacol.* **216**, 139-140.

Prast, H., Tran, M. H., Fischer, H. and Philippu, A. (1998). Nitric oxide-induced release of acetylcholine in the nucleus accumbens, role of cyclic GMP, glutamate, and GABA. *J. Neurochem.* **71**, 266-273.

Prast, H., Fischer, H., Werner, E., Wernerfelmayer, G. and Philippu, A. (1995). Nitric oxide modulates the release of acetylcholine in the ventral striatum of the freely moving rat. *Naunyn Schmiedebergs Arch. Pharmacol.* **352**, 67-73.

Radomski, M. W., Martin, J. F. and Moncada, S. (1991). Synthesis of nitric oxide by the hemocytes of the American horseshoe crab (*Limulus polyphemus*) *Phil. Trans. R. Soc. Lond. B.* **334**, 129-133.

Regulski, M. and Tully, T. (1995). Molecular and biochemical characterization of dNOS: a *Drosophila* Ca^{2+}/calmodulin-dependent nitric oxide synthase. *Proc. Natl. Acad. Sci. USA* **92**, 9072-9076.

Rewitz, K. F., Yamanaka, N. and O'Connor, M. B. (2013). Developmental checkpoints and feedback circuits time insect maturation. In *Animal Metamorphosis*, vol. 103 (ed. Y. B. Shi), pp. 1-33.

Ribeiro, J. M. C., Hazzard, J. M. H., Nussenzveig, R. H., Champagne, D. E. and Walker, F. A. (1993). Reversible binding of nitric oxide by a salivary heme protien from a bloodsucking insect. *Science* **260**, 539-541.

Roman, L. J., Martasek, P. and Masters, B. S. S. (2002). Intrinsic and extrinsic modulation of nitric oxide synthase activity. *Chem. Rev.* **102**, 1179-1189.

Rudolph, P. H. and Spaziani, E. (1991). Neurons demonstrable by nickel lysine backfilling of the optic peduncle in the crab *Cancer antennarius*. *Comp. Biochem. Physol.* **99C**, 179-184.

Russwurm M., **Russwurm C., Koesling D., Evanthia M.** (2013). NO/cGMP: The past, present, and the future. *Methods in Molec. Biol.* **1020**, 1-16.

Scholz, N. L. (1999). NO/cGMP signaling and the specification of motor networks in the crab stomatogastric ganglion. *Am. Zool.* **39**, 46A-46A.

Scholz, N. L., Chang, E. S., Graubard, K. and Truman, J. W. (1998). The NO/cGMP pathway and the development of neural networks in postembryonic lobsters. *J. Neurobiol.* **34**, 208-226.

Scholz, N. L., Labenia, J. S., De Vente, J., Graubard, K. and Goy, M. F. (2002). Expression of nitric oxide synthase and nitric oxide-sensitive guanylate cyclase in the crustacean cardiac ganglion. *J. Comp. Neurol.* **454**, 158-167.

Schuppe, H., Cuttle, M., Chad, J. E. and Newland, P. L. (2002). 4,5-Diaminofluoroscein imaging of nitric oxide synthesis in crayfish terminal ganglia. *J. Neurobiol.* **53**, 361-369.

Schwarz, P. M., Rodriguez-Pascual, F., Koesling, D., Torres, M. and Forstermann, U. (1998). Functional coupling of nitric oxide synthase and soluble guanylyl cyclase in controlling catecholamine secretion from bovine chromaffin cells. *Neurosci.* **82**, 255-265.

Sequeira, S. M., Ambrosio, A. F., Malva, J. O., Carvalho, A. P. and Carvalho, C. M. (1997). Modulation of glutamate release from rat hippocampal synaptosomes by nitric oxide. *Nitric Oxide-Biol. Ch.* **1**, 315-329.

Skinner, D. M. (1985). Molting and regeneration. In *The Biology of Crustacea*, vol. 9 eds. D. E. Bliss and L. H. Mantel), pp. 44-146. New York: Academic Press.

Stasiv, Y., Regulski, M., Kuzin, B., Tully, T. and Enikolopov, G. (2001). The *Drosophila* nitric oxide synthase gene (dNOS) encodes a family of proteins that can modulate NOS activity by acting as dominant negative regulators. *J. Biol. Chem.* **276**, 42241-42251.

Stuenkel, E. L. (1985). Simultaneous monitoring of electrical and secretory activity in peptidergic neurosecretory terminals of the crab. *J. Physiol. Lond.* **359**, 163-187.

Virarkar, M., Alappat, L., Bradford, P. G. and Awad, A. B. (2013). L-arginine and nitric oxide in CNS function and neurodegenerative diseases. *Crit. Rev. Food Sci. Nutr.* **53**, 1157-1167.

Vitecek, J., Reinohl, V. and Jones, R. L. (2008). Measuring NO production by plant tissues and suspension cultured cells. *Molec. Plant* **1**, 270-284.

Weichsel, A., Maes, E. M., Andersen, J. F., Valenzuela, J. G., Shokhireva, T. K., Walker, F. A. and Montfort, W. R. (2005). Heme-assisted S-nitrosation of a proximal thiolate in a nitric oxide transport protein. *Proc. Natl. Acad. Sci. USA* **102**, 594-599.

Wilson, M. T. and Torres, J. (2004). Reactions of nitric oxide with copper containing oxidases; Cytochrome c oxidase and laccase. *Iubmb Life* **56**, 7-11.

Wu, C. H., Siva, V. S. and Song, Y. L. (2013). An evolutionarily ancient NO synthase (NOS) in shrimp. *Fish Shellfish Immunol.* **35**, 1483-1500.

Yao, C. L., Ji, P. F., Wang, Z. Y., Li, F. H. and Xiang, J. H. (2010). Molecular cloning and expression of NOS in shrimp, *Litopenaeus vannamei*. *Fish Shellfish Immunol.* **28**, 453-460.

Yeh, F. C., Wu, S. H., Lai, C. Y. and Lee, C. Y. (2006). Demonstration of nitric oxide synthase activity in crustacean hemocytes and anti-microbial activity of hemocyte-derived nitric oxide. *Comp. Biochem. Physol.* **144B**, 11-17.

Zou, H. S., Chang, Y. Z., Chen, S. C., Yau, S. M., Shen, Y. L. and Lee, C. Y. (2002). Localization of NADPH-diaphorase and nitric oxide synthase activity in the eyestalk of the crayfish, *Procambarus clarkii*. *Zool. Stud.* **41**, 244-250.

Figure Legends

Fig. 1. Tissue expression of *Cm-NOS* and *Cm-EF2* using end-point RT-PCR. PCR products (158 bp for *Cm-NOS* and 278 bp for *Cm-EF2*) were separated on a 1.5% agarose gel and stained with ethidium bromide (inverted images). *Cm-EF2* was expressed in all tissues. *Cm-NOS* was expressed in all tissues except heart (Ht) and hepatopancreas (Hp). Other abbreviations: CM, claw muscle; TM, thoracic muscle; Gi, gill; Hg, hindgut; Mg, midgut; Br, brain; TG, thoracic ganglion; ESG, eyestalk ganglia; Te; testes; W, water (no template control).

Fig. 2. Western blot analysis of Cm-NOS protein in the sinus gland. SG soluble protein was separated by SDS-PAGE, transferred to PVDF membrane, and probed with (Lane a) or without (Lane b) universal NOS antibody. Detection of primary antibody used a goat anti-rabbit IgG plus ABC reagent and chemiluminescence (see Materials and Methods). The primary antibody recognized a protein of the predicted mass ~132-kDa for Cm-NOS and a second protein (~94 kDa), which may represent an uncharacterized truncated NOS isoform. Protein standards, with approximate masses, are shown in the left panel.

Fig. 3. Localization of NO-FL in the sinus gland *in situ*. (A) Whole ESG was preincubated with crab saline for 30 min and loaded with 0.05 µM CuFL for 1 h in the dark. Stacked images were obtained with a scanning laser confocal microscope at 10x magnification (scale bar = 200 µM). SG; sinus gland MI: medulla interna.

Fig. 4. Effects of cPTIO and L-NAME on NO-FL fluorescence in the sinus gland during the preincubation period. SGs were preincubated with saline, 1 mM cPTIO alone, or cPTIO in combination with 1 mM L-NAME for 30 min and loaded without or with 0.05 µM CuFL for 1 h in the dark. (A) Total NO-FL fluorescence (mean ± 1. s.e., n = 6). Gray-shaded columns compare relative fluorescence intensity between SG pairs preincubated in crab saline and loaded with or without CuFL. Open columns compare fluorescence between SG pairs preincubated with or without cPTIO and loaded with CuFL. Black-filled columns compare fluorescence between SG pairs preincubated with or without cPTIO and L-NAME. Significant differences, with p value, between SG pairs are indicated by horizontal lines. Numbers on the columns correspond to the confocal microscope images in (B). (B) Representative confocal images of SGs. Panels 1, 2, 3,

and 4 correspond to the column numbers in (A). All images were taken on a scanning laser confocal microscope at 10x (scale bar = 200 µM).

Fig. 5. Effects of L-NAME, cPTIO, and NaN_3 on NO-FL fluorescence in the sinus gland. SGs were preincubated with saline or the indicated compound(s) for 30 min and loaded with 0.05 µM CuFL plus the indicated compound(s). The concentration of cPTIO, L-NAME, and NaN_3 was 1 mM. (A) Total NO-FL fluorescence (mean ± 1. s.e.). Light gray-shaded columns compare fluorescence between SG pairs preincubated with saline and loaded with CuFL without or with cPTIO (n = 9). Open columns compare fluorescence between SG pairs preincubated with cPTIO and loaded with CuFL without or with cPTIO (n = 12). Black-filled columns compare fluorescence between SG pairs preincubated with cPTIO and L-NAME and loaded with CuFL without or with L-NAME (n = 10). Dark gray-shaded columns compare fluorescence between SG pairs preincubated with cPTIO + L-NAME without or with NaN_3 and loaded with CuFL with L-NAME (n = 6). Significant differences, with p value, between SG pairs are indicated by horizontal lines. Numbers in the columns correspond to the confocal images in (B). (B) Representative confocal images of SGs. Panels 1, 2, 3, and 4 correspond to the column numbers in (A). All images were taken on a scanning laser confocal microscope at 10x (scale bar = 200 µM).

Fig. 6. Effects of sodium azide and 70% methanol on SG cell viability. SG were incubated with crab saline, 1 mM NaN_3, or 70% methanol for 30 min, stained with propidium iodide (indicated with green) and Hoechst (indicated with red) stains, and imaged by confocal microscopy (see Materials and Methods). The nuclei of glial and other supportive cells were stained. Groups of axon termini were located in regions lacking nuclei (arrows). Dead cells were identified by nuclei stained with both propidium and Hoechst (orange to yellow) in overlay images. Scale bar = 100 µM.

Fig. 7. Effect of sodium azide on absorption spectra of soluble proteins from the sinus gland. Top panel shows the spectra of the SG extract prior to the addition of NaN_3 (red line – no azide) and immediately after the addition of 1 mM NaN_3 (green line – 0 min). Bottom panel shows spectral shifts at 5-min intervals after the addition of NaN_3. Spectra at 0 to 60 min are the

differences between the baseline spectrum (no azide) and the spectrum at a specific time point. A positive spectral shift occurred at ~225 nm (black arrow) and a negative spectral shift occurred at ~255 nm (white arrow).

Fig. 8. Schematic diagram summarizing the effects of L-NAME, cPTIO, and NaN_3 on NO production, sequestration, and degradation in the sinus gland. NOS produces NO, which binds NO-dependent proteins (not shown) or is sequestered by NO-binding protein (XX-NO). NO scavenger cPTIO converts NO to NO_2. CuFL reacts with NO, reducing Cu (II) to Cu (I), to produce highly fluorescent NO-FL. L-NAME decreases NO-FL fluorescence by inhibiting NOS. cPTIO decreases NO-FL fluorescence during preincubation, but is out-competed by CuFL during the loading period. Preincubation of SGs with NaN_3 displaces NO from the NO-binding protein (N_3XX) and the NO combines with water to form nitrite and nitrate. Maximum reduction of NO-FL fluorescence is achieved when the SG is preincubated with L-NAME, cPTIO, and NaN_3 and when L-NAME is included during CuFL loading.

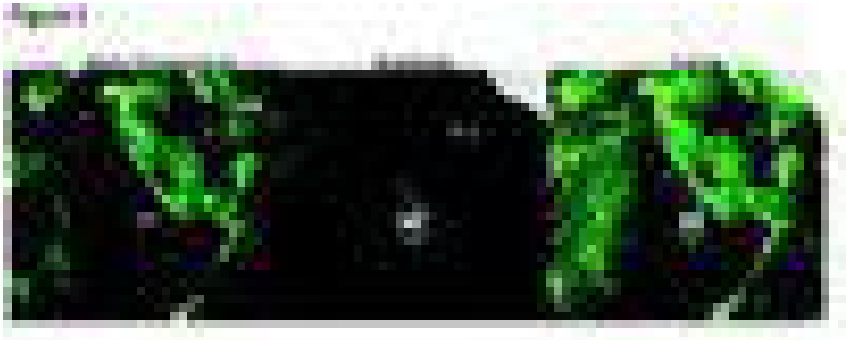

Figure 4A

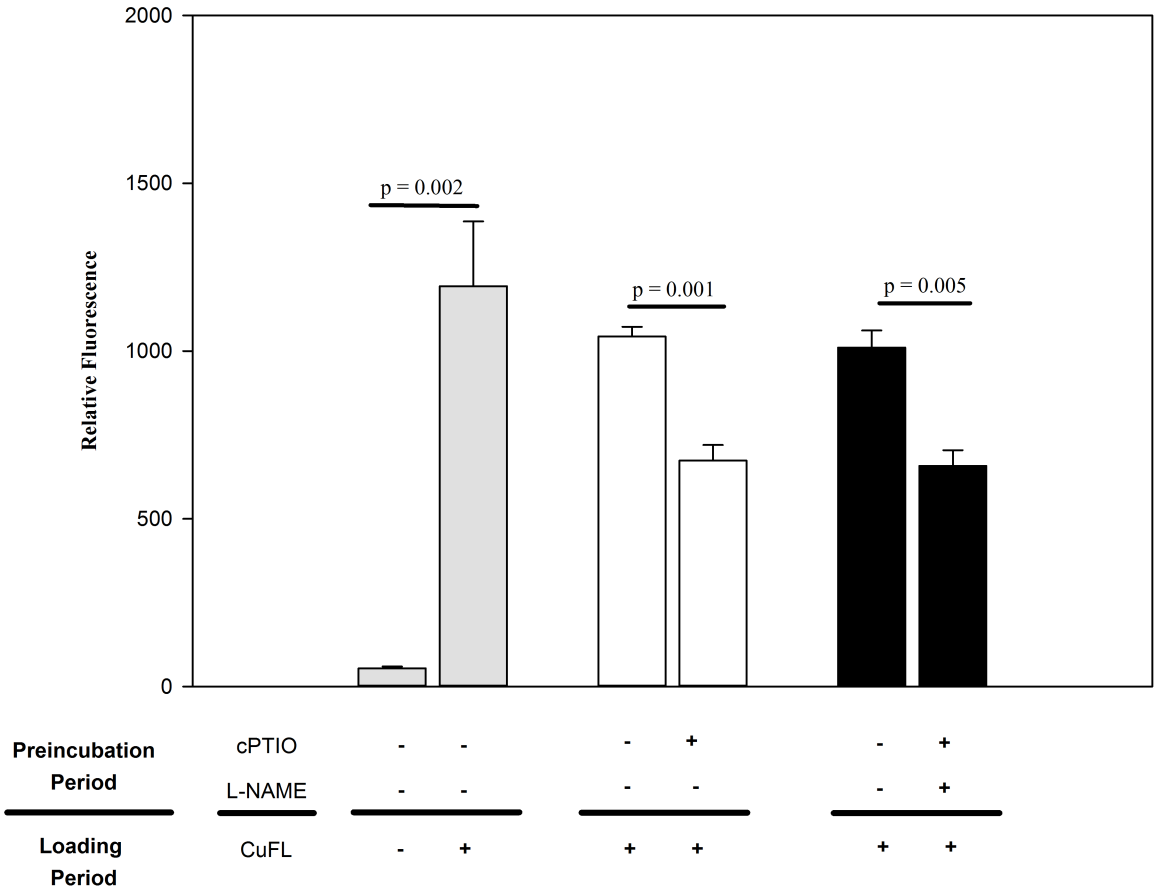
2000
1500
1000
500
0
Relative Fluorescence
p = 0.002
p = 0.001
p = 0.005
Preincubation Period
cPTIO - - - + - +
L-NAME - - - - - +
Loading Period
CuFL - + + + + +

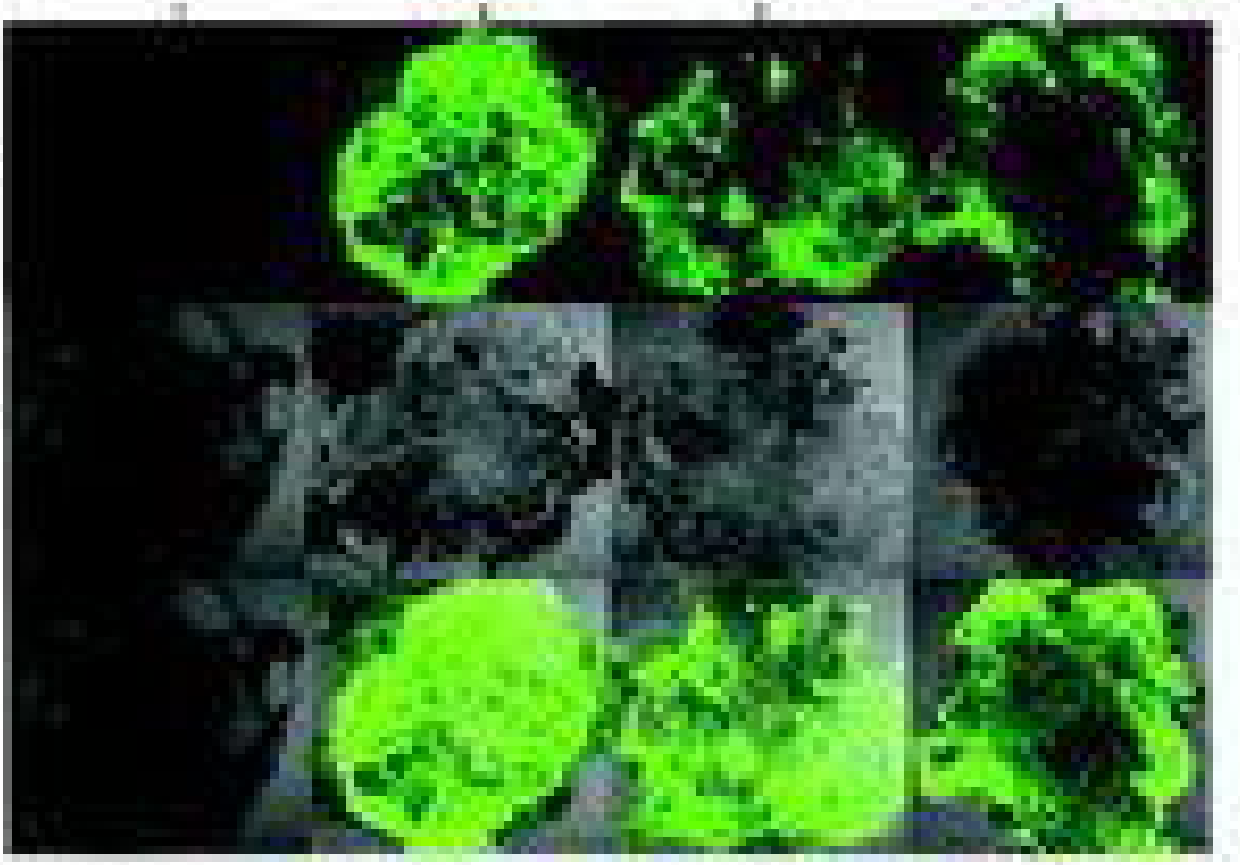

Figure 5A

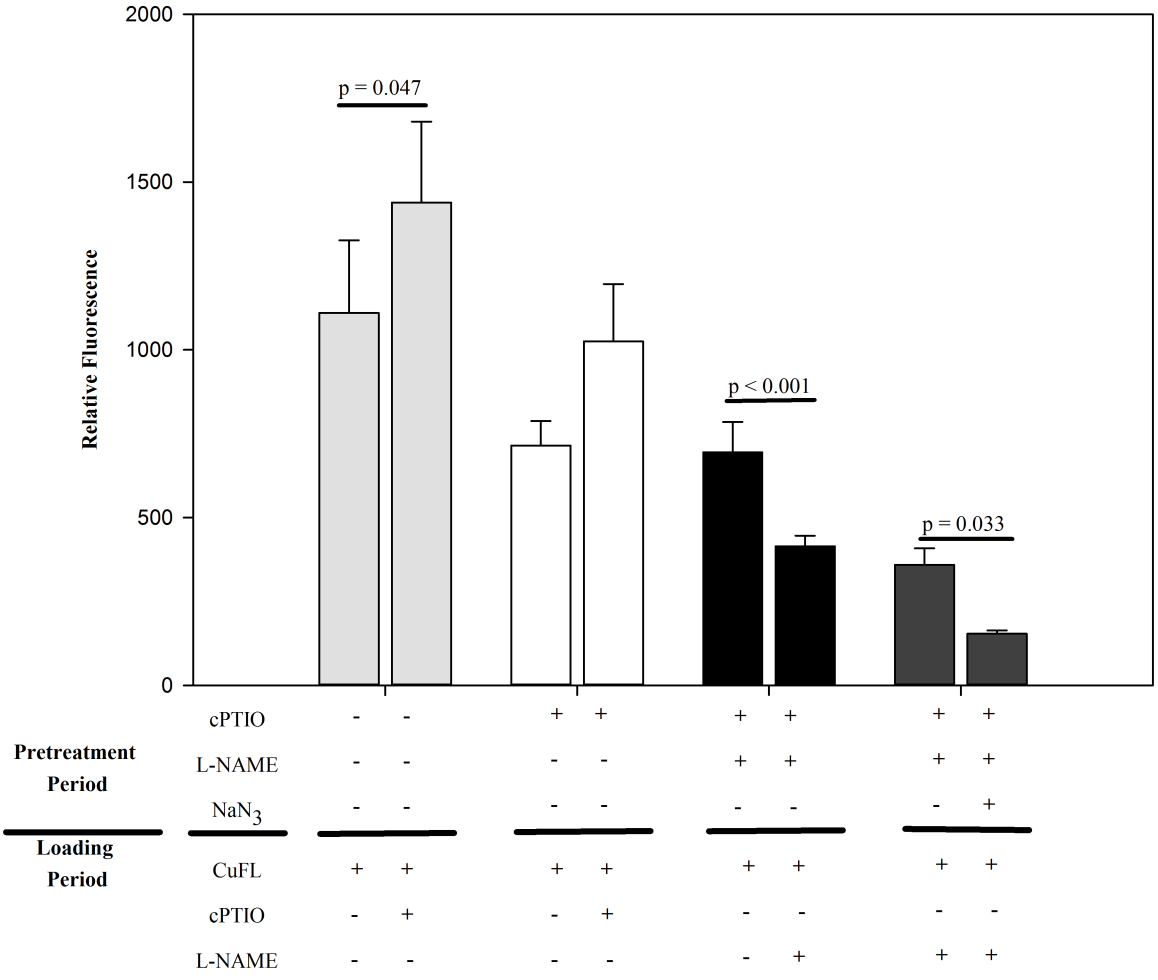
2000
1500
1000
500
0
Relative Fluorescence
p = 0.047
p < 0.001
p = 0.033
Pretreatment Period
cPTIO - - + + + + + +
L-NAME - - - - + + + +
NaN3 - - - - - - - +
Loading Period
CuFL + + + + + + + +
cPTIO - + - + - - - -
L-NAME - - - - - + + +

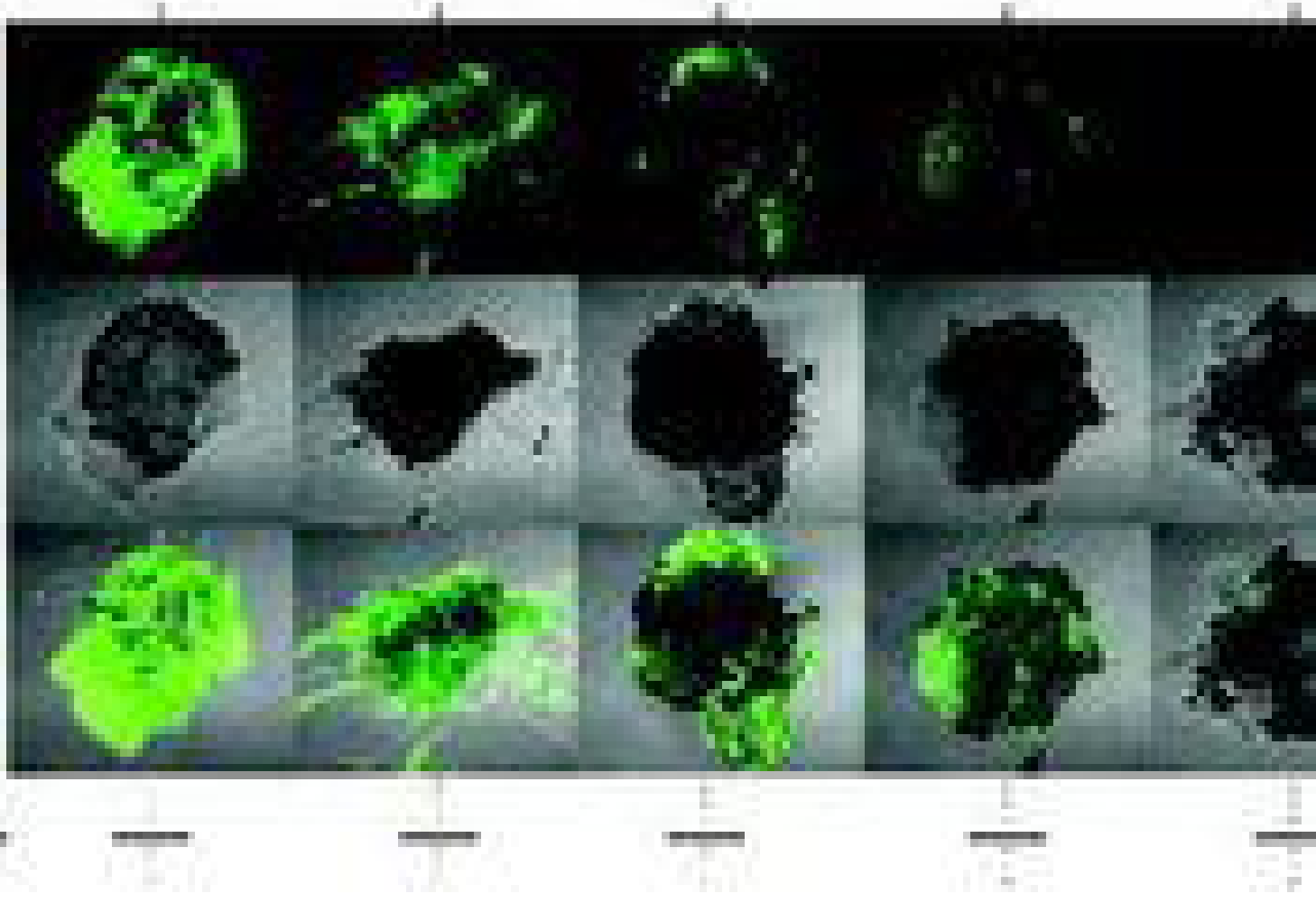

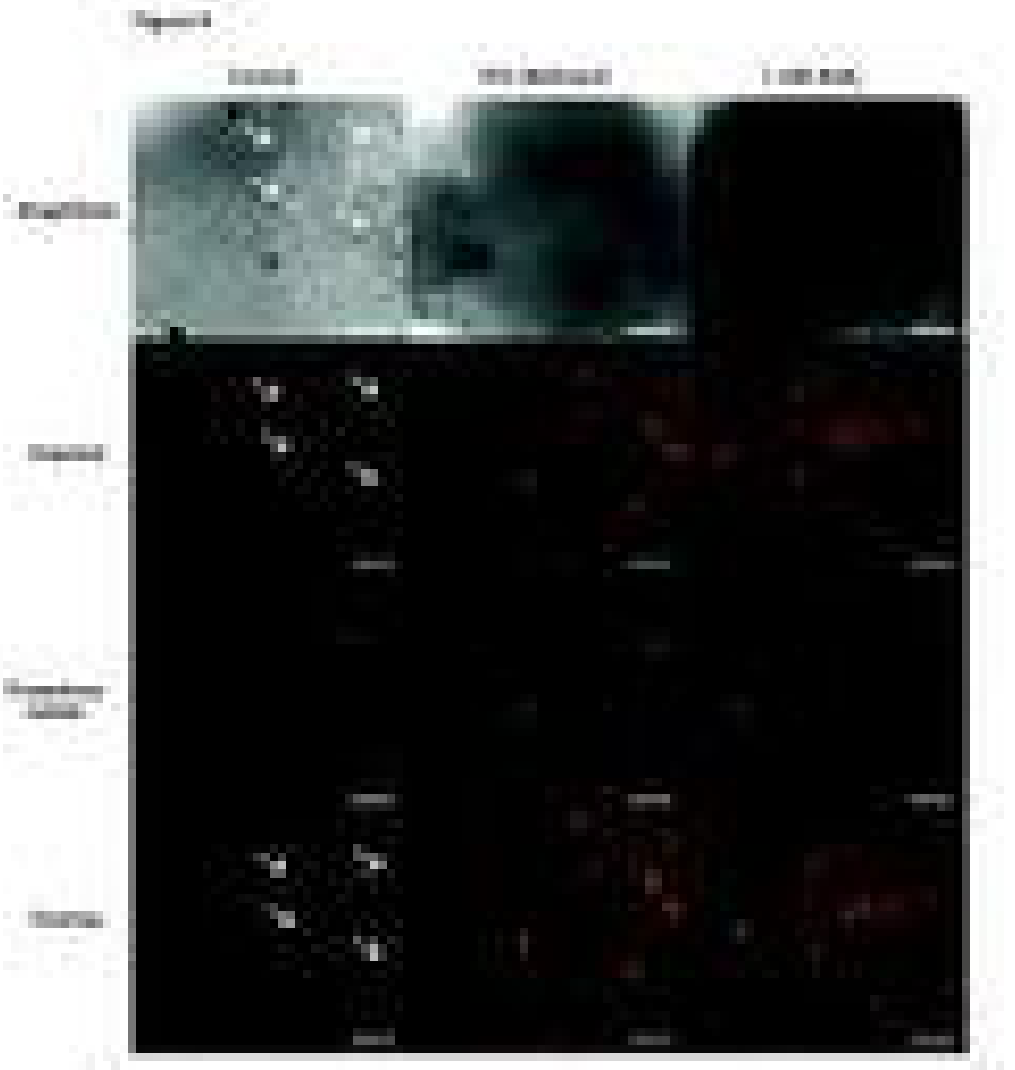

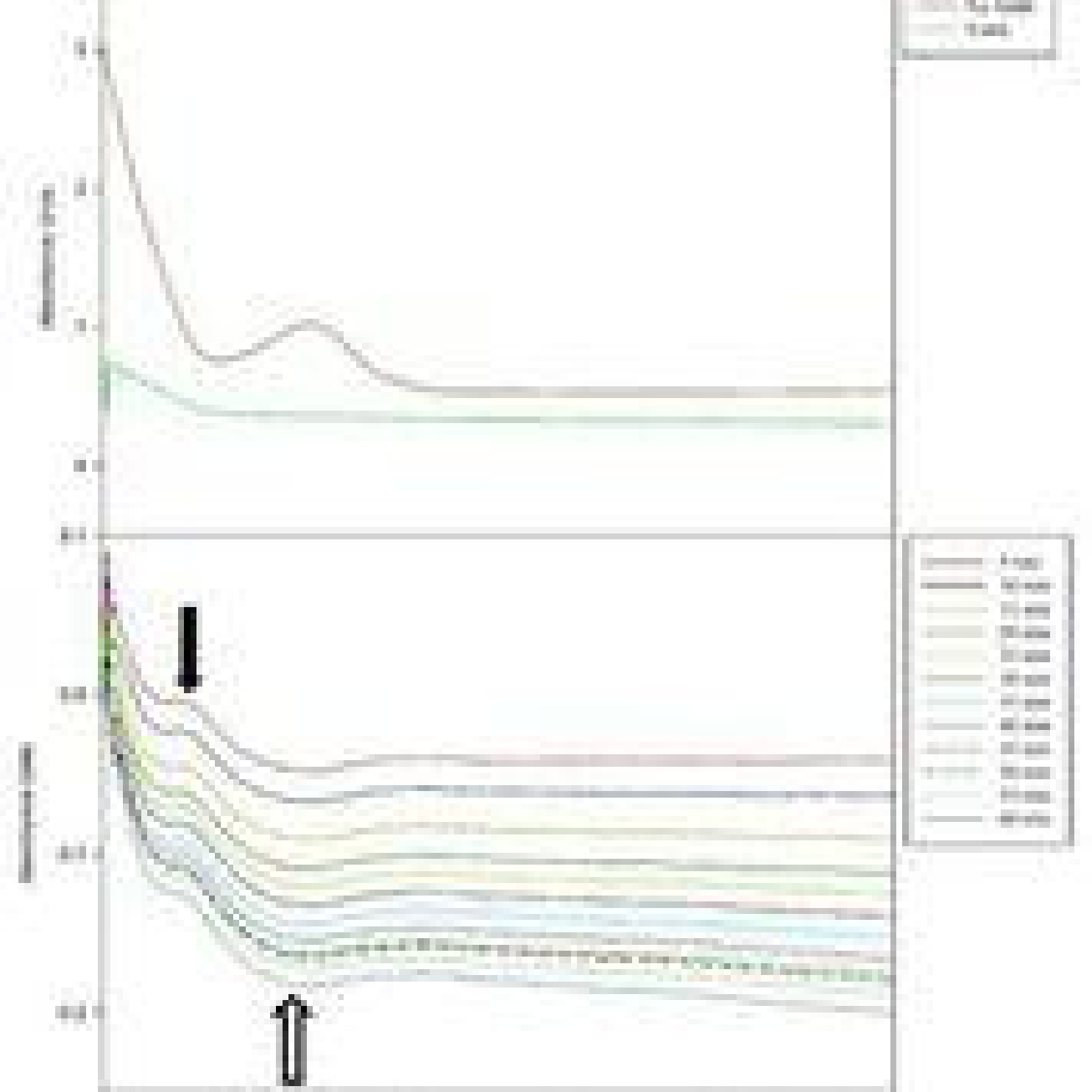

Figure 8

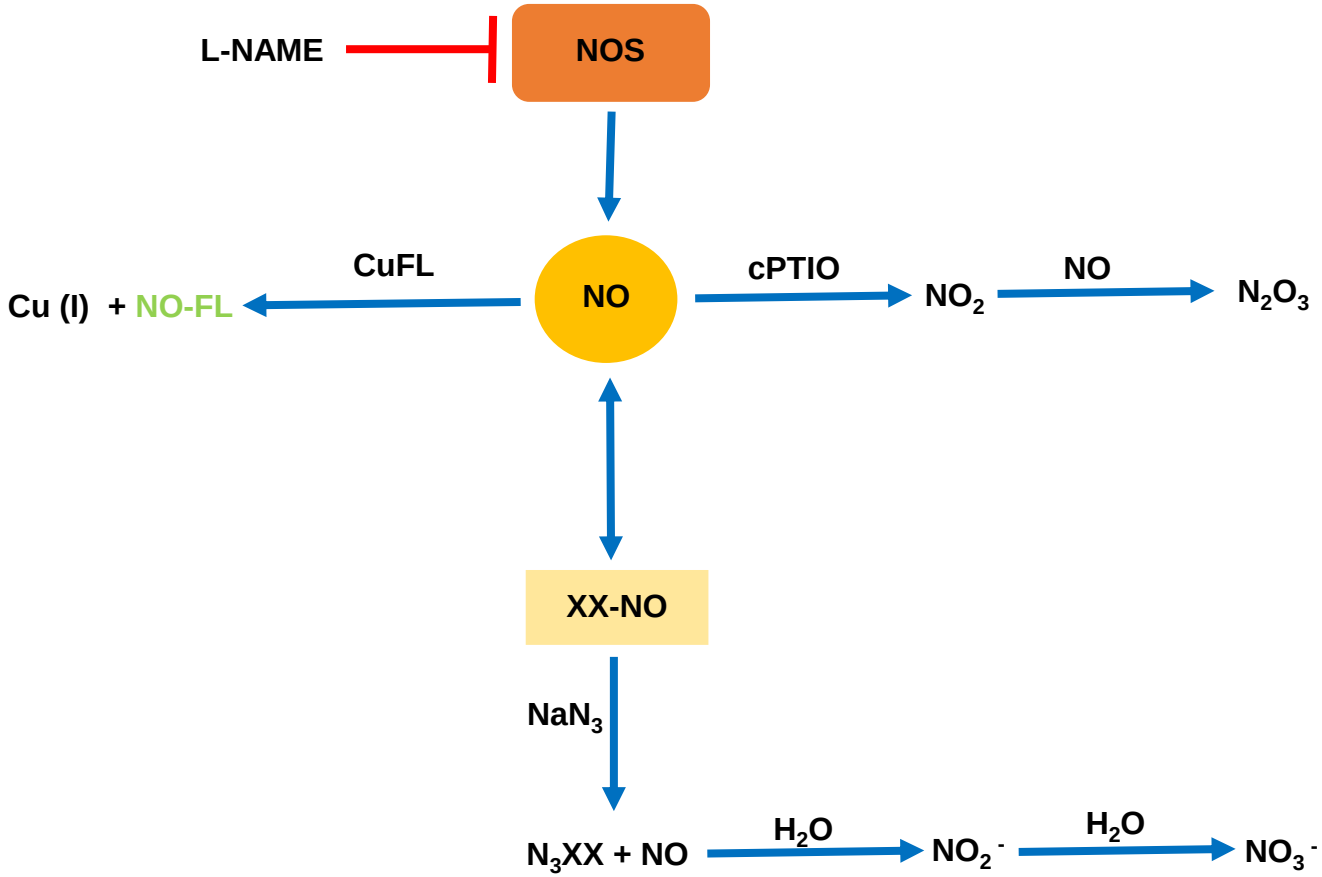
L-NAME
NOS
CuFL
Cu (I) + NO-FL
NO
cPTIO
NO2
NO
N2O3
XX-NO
NaN3
N3XX + NO
H2O
NO2 -
H2O
NO3 -